Reference No. Th.I-01

Experimental Studies of Electrons in a Heavy-Ion Beam

A. W. Molvik[a], M. Kireeff Covo [a], F. M. Bieniosek[b], R. H. Cohen[a], A. Faltens[b], A. Friedman[a], S. M. Lund[a], L. Prost [b], P. A. Seidl[b]

Heavy Ion Fusion Virtual National Laboratory,

[a] Lawrence Livermore National Laboratory, Livermore, CA 94550, USA.

[b] Lawrence Berkeley National Laboratory, Berkeley CA 9472-82010, USA

Abstract

We have measured electron and gas emission from 1 MeV K^+ impact on surfaces near grazing incidence on the High-Current Experiment (HCX) at LBNL. Electron emission coefficients reach values of 130, whereas gas desorption coefficients are near 10^4. Mitigation techniques are being studied: A bead-blasted rough surface reduces electron emission by a factor of 10 and gas desorption by a factor of 2. Diagnostics are installed on HCX, between and within quadrupole magnets, to measure the beam halo loss, net charge and expelled ions, from which we infer gas density, electron trapping, and the effects of mitigation techniques. Here we discuss a new diagnostic technique that measures gas pressure and electron ionization rates within quadrupole magnets during the beam transit.

PACS: 29.27.Bd, 34.50.Dy, 52.70.NC, 52.58.Hm

Keywords: Electron cloud, mitigation, pressure rise, pressure measurement

Corresponding Author:

Arthur Molvik
L-637
LLNL
Livermore, CA 94550

Tel. 925-422-9817
Fax 925-424-6401
E-mail molvik1@llnl.gov

1. Introduction

Electron cloud effects (ECEs) [1] and beam-induced pressure rises [2], that are frequently observed to limit the performance of colliders and high-intensity rings, are normally a problem only in ring accelerators. However, the cost of future high-intensity accelerators for Heavy Ion Inertial Fusion (HIF) and High Energy Density Physics (HEDP) can be reduced by fitting beam tubes more tightly to beams. This places them at risk from gas desorption runaway, and from electron clouds produced by secondary electrons and ionization of gas [3]. We are engaged in an experimental and theoretical program to measure, understand, and model these effects in heavy-ion accelerators [4,5]. In this paper, we review measurements of ion induced electron emission and gas desorption for ions near grazing incidence, discuss a mitigation technique [6], and discuss measurements using diagnostics inside quadrupole magnets to measure local densities of gas, and the rate of electron generation from ionization of gas.

Residual-gas beam-profile monitors, which are related to our gas density diagnostic, have been demonstrated previously. Beam impact on residual gas produces ion-electron pairs and causes excitation of the gas molecules. Any of these interaction products can be measured to obtain the gas density; or by using multiple spatially distributed channels, the beam profile can be obtained. Many of these monitors use an electric field parallel to a dipole magnetic field (both normal to the beam) to direct electrons from residual gas to a multichannel plate (MCP) detector [7,8,9]. In these, the applied electric field dominates over the beam self field, the magnetic field is large enough to confine electrons to orbits much less than the beam radius for adequate spatial resolution, and the MCP provides high gain enabling profiles of beams with low current (of order 1 mA or lower) to be measured in ultra-high vacuum (UHV). The beam profile is the main result, however the peak of the profile or the integration of the signal over the beam profile can be calibrated to yield the residual gas density. Others have used fluorescence of excited residual gas [10] or of an injected gas sheet [11] to obtain the beam profile; the former could also determine the residual gas pressure.

Our device differs in several ways: (a) It depends on the positive beam self field to expel cold ions from beam impact on residual gas, rather than using an applied electric field to drive electrons from beam impact on residual gas into a detector. Our technique has the advantage of not perturbing the low-energy ion beam, but it misses ~90% of the expelled ion current because the ions are expelled radially and our collector subtends only a small fraction of the circumference. (b) Our technique collects expelled ions directly rather than amplifying the electron current with an MCP in either an analog or counting mode – this restricts our operation to high vacuum rather than UHV but, for the beam parameters discussed below, provides response times of 0.5-1.5 μs. This is the time for the unneutralized beam potential of 300-2000 V to expel a cold oxygen ion. Hydrogen ions are expelled more quickly, in 0.1-0.4 μs. These times are substantially less than the beam FWHM of 5 μs, and so indicate the capability of measuring the time dependence of desorbed gas reaching the beam. (c) A consequence of

(a) and (b) is that we measure the residual gas density, but cannot obtain the beam profile. (d) Our technique collects expelled ions across a quadrupole magnetic field rather than collecting electrons along a dipole magnetic field. This enables the magnetic field to suppress electron emission from the collector, while keeping the field low enough for ions to cross it. The requirement that expelled ions cross the quadrupole field restricts our technique to beams with relatively high space charge and low beam energy (for low quadrupole field strength), so that the beam potential provides sufficient energy to drive ions across the quadrupole magnetic field, and MCPs will not function in the transverse magnetic field. Item (d) is not essential to our concept: we are designing a retarding potential analyzer to be inserted into a magnetic-field-free drift region between magnets, where we could also relax feature (a) by applying an electric field to drive all ions from gas into the analyzer. This is intended to measure both the gas density, from the total current of expelled ions in the beam, and the beam potential, from the expelled-ion energy, as a function of time.

On the High-Current Experiment (HCX) we are using a 1 MeV, 180 mA, K^+ ion beam to study transport [12], beam induced electron emission and gas desorption [6], and electron cloud and gas effects in magnetic quadrupoles [4,5]. The beam has a space-charge potential of ~2 kV, rise and fall times of 0.3 and 1 μs respectively, and a flattop duration of 4 μs, and is pulsed at 10 s intervals. An aperture can be inserted at the diagnostic region immediately preceding the magnetic quadrupoles, to reduce the beam current to 25 mA and ~300 V space-charge potential. Electron transit times between walls are in the range of 7 ns (20 ns if apertured) for an unneutralized beam, almost 3 orders of magnitude shorter than the flattop duration. This enables exploration of unique electron trapping regimes: multipactor trapping will not occur during the flattop, and trailing edge multipactor is not an issue because any electrons generated will be lost before the next pulse in ~10 s. However electrons, emitted from the wall under beam bombardment, will be trapped during the current rise at the beam head. Ionization of gas by the beam also generates electrons that are deeply trapped while the associated ions from gas are expelled by the positive beam potential, in Section 3 we will discuss exploiting ion expulsion to measure gas density and electron generation.

2. Mitigation of electron and gas emission

Electron emission and gas desorption coefficients η_e and η_0 respectively, due to ion bombardment of metal surfaces near grazing incidence, have been measured with the Gas-Electron Source Diagnostic (GESD). This information enables us to interpret electron emission currents from electrodes in beam tubes in terms of the beam-halo loss that caused the emission, and to infer the resulting gas desorption. We find that η_e ~ 10^2 and η_0 ~10^4 for 1 MeV K^+ ions incident on stainless steel [6]. The electron emission coefficient is shown in Fig. 1(a). The dependence of the electron emission coefficient η_e on the ion angle of incidence, relative to normal, is observed to scale as η_e 1/cos(θ), where d/cos(θ) is the ion path length through a thin d ≈ 2 nm thick surface

layer (from which the emitted electrons originate). Similar scaling was observed at higher ion energies by Thieberger [13].

The gas desorption coefficient η_0, is measured from the pressure rise of the 4 l volume of the GESD after a pulse. The GESD pumps out through the 0.3 by 2.5 cm entrance aperture, plus a 1 cm diameter hole, giving a pump-out time constant of 0.3 sec, long enough for an ion gauge to determine the peak pressure, but short compared with the 10 s before the next pulse. The less than $1/\cos(\theta)$ dependence of gas desorption indicates that it is not only from layers of gas adsorbed on the surface (Fig. 1(b)). Similar scaling with the ion angle of incidence was observed at higher ion energies by Mahner [14].

Beam halo loss in magnetic quadrupoles occurs at the maximum excursion of the beam envelope, near the major diameter; without ion scattering any electrons emitted from the wall are confined close to the wall (every 90°) by the quadrupole magnetic field. Ion scattering from the surface exacerbates the emission and desorption, not only allowing ions to impact a surface multiple times, but also allowing them to impact the wall in regions from which the quadrupole magnetic field passes through the beam. We have evaluated ion scattering using the SRIM (TRIM) Monte Carlo code [15], which predicts that 75% of 1 MeV K^+ ions reflect (called backscatter in the code) when incident at 88-89°. from normal [6]. The median lateral angle of scattered ions is near 4° and 6° for ions incident at 89° and 88° respectively, but a few ions scatter through angles up to 90°. The angular distribution of scattered ions can be approximated by two exponentials: the first factor of ~7 decay has an e-folding of 4-6°, subsequently decaying with an e-folding of about 13°. [A power law does not fit better than the two exponentials.] The scattered ions generate electrons from all around the wall that fill the entire quadrupole magnet, as contrasted with ion-induced electrons that are confined near the wall by the magnetic field in the absence of ion scattering, in the simulation of Cohen [16,17]. This broad angular distribution of scattered ions also complicates suppression of electron emission from grids and electrodes of diagnostics. These could be shielded from near-grazing halo ions by low beam scrapers, but scrapers of any height are only partially effective at removing the scattered ions.

The GESD is also useful for studying mitigation techniques as evidenced by Fig. 1. Based on the observation that ion scattering decreases rapidly away from grazing incidence (by an e-fold every 8.5° [6]) as well as on the observation that electron emission scales as $1/\cos(\theta)$, we tried roughening a surface using glass bead blasting. (This was intended to result in most grazing-incidence ions striking the rims of craters on the roughened surface at angles closer to normal incidence.) The surface appears to have undergone fine-grained sandblasting. The approximate scale length of the roughness of the surface is 100 μm. We characterized the target roughness, before installing it in the GESD apparatus, by measuring the spot size of reflected light from a laser at near normal incidence onto the target. The bright spot indicated half angles of 17°, out to about 23° for fainter light. However, this technique over emphasizes the bottoms of craters, which may be relatively flat, whereas ions near grazing incidence will preferentially

strike the rim of the craters, which are likely to be steeper. Since electron emission from a smooth surface was well fit by 6.06/cos(□), we infer an angle of 62° relative to normal from the emission coefficient of 12.8 off the rough surface in Fig. 1(a). The change in gas desorption in Fig. 1(b) is not inconsistent with such an angle from an empirical extrapolation of the measured dependence on angle back to about 60°, although we don't have a model for how this should vary. The effect of roughened surfaces on ion scattering is based entirely on the SRIM code at present (the ion scattering predictions have not been benchmarked). At 60° the predicted ion backscattering is 3%, down a factor of 25 from the 75% near grazing incidence.

3. Gas and electrons in magnetic quadrupoles

The HCX in the region of four magnetic quadrupoles is shown in Fig. 2. To the left is the D2 diagnostic region between 10 electrostatic quadrupoles and the 4 magnetic quadrupoles. Each magnetic quadrupole has 30 cm long magnetic field coils in a 47 cm length elliptical tube that has minor and major inner radii of 3 cm and 5 cm respectively. Between each pair of magnets, and after the last one, diagnostic access is provided in a 5 cm gap, each with 7 ports. Arrays of diagnostics are mounted on octagonal tubes that fit the elliptical beam tube bore in the third and fourth quadrupoles. A gap of about 0.7 cm annular space is provided between the octagonal diagnostics mounting tube and the elliptical magnet bore for the recessed diagnostics and cables. These diagnostics include capacitive electrodes to measure the net beam charge, electrodes shielded from the beam electric field by grids to measure the current of expelled ions from gas ionization in the fourth quadrupole, and flush electrodes running the length of the octagonal tube in the third quadrupole divided azimuthally into two per quadrant. Electron-clearing ring electrodes are inserted in the drift regions between quadrupole magnets, and can be biased to +10 kV to remove electrons from the drift regions between magnets. Another ring electrode surrounding the beam between the exit of the last quadrupole magnet and the downstream diagnostics can be biased to −10 kV to suppress beam-induced electrons, generated on the end structures, from reaching the magnets [18].

For initial tests of the diagnostics in magnetic quadrupoles, we aperture the beam at D2 to reduce the beam halo near the walls. This reduces the full beam current of 180 mA to about 25 mA.

A pair of gridded electrodes are located on the minor axis of the octagonal tube in the fourth magnet where the quadrupole magnetic field is tangent to the electrode surface, such that it can suppress electron emission or collection by the electrode. The grids are electroplated mesh from Buckbee Mears, 35 mesh/cm, 88% transmission, ~5 μm thick nickel, that are sandwiched between 0.25 mm thick stainless steel frames and spot welded around the periphery of the aperture (0.7 x 10 cm). Two grids, separated by 0.25 mm are used to improve the shielding of the electric field of the beam. (Two grids provide a factor of ~20 times better shielding than a single grid.) Bench tests performed by pulsing a square wave onto a 2.5 cm diameter metal rod

through the center of the diagnostics tube demonstrated that the shielding reduced the capacitive signal to the two shielded electrodes by factors exceeding 600 times compared to an unshielded capacitive electrode scaled to the same aperture area.

The gridded electrode is biased at –50 V. The current varies by only 12% as the bias is varied from -30 to -80 V; this saturation of the current indicates a reliable measurement. The quadrupole magnetic field provides magnetic insulation to prevent electrons from flowing between the grids and the electrode. Ions, however, are driven across the magnetic field ($B' \sim 8$ T/m) by the beam potential. Singly ionized argon can be expelled across the field with a (partially-neutralized) beam potential as low as 35 V. With an unneutralized, apertured beam potential of 300 V, ions as low in mass as 5 amu can reach the electrode.

With the apertured beam, we observe currents that ramp from 0.6 to ~2 μA to each gridded electrode, as shown in Fig. 3(a). This pulse shape is reasonable: the initial value appears to represent the base pressure, and the ramping could be due to desorbed gas reaching the beam within the fourth magnet. We test this hypothesis by injecting argon gas into the gap between magnets 3 and 4, thereby varying the base pressure with a known gas. We find that the initial current, at the beginning of the beam pulse, increases with the gas pressure; and that the ramping of current, after the initial fast rise, continues to rise by ~1.5 μA at the end of each pulse for gas densities up to 8×10^{10} cm^{-3}. This is consistent with the beam loss to the wall (and the resulting gas desorption) not varying over a factor of 10 in gas pressure. We calculate the gas pressure at the center of the gridded electrodes within magnet 4, from measurements made with a cold cathode ionization gauge between magnets 3 and 4 and a Bayard-Alpert ionization gauge in D-End. We assume that the pressure decreases linearly through the fourth magnet, and determine that the gridded electrode is 37% of the way upstream towards drift region (c). We correct for argon gas with the manufacturer's correction factor of 0.8 relative to air. Then

$$P(\text{effective}) = 0.37[P_{base} + 0.8(P_{34} - P_{base}) - P_{end}] + P_{end}$$

For Fig. 3(b), we convert pressure to the density of molecules with the factor 3.3×10^{16} molecules/(cm^3 torr).

We estimate the fractional volume of the beam that expels ions into a gridded electrode from the geometry: the electrode aperture is 0.7 cm x 9.8 cm long at a minor radius of 2.4 cm. From an envelope code, we determine that the major radius is approximately twice the minor radius. Then the pie-slice of beam viewed is 0.023 of the total beam volume in that 9.8 cm length. From a particle balance for expelled ions

$$dn_i/dt = n_b\, n_0\, v_b\, \sigma_{I+cx}$$

where n_i is the density of expelled ions, n_b the beam ion density, v_b the beam velocity, and σ_{I+cx} the sum of the cross sections for charge exchange and ionization of gas by beam impact. We multiply dn_i/dt by an electron charge and by the volume of beam viewed (1.06 cm^3 for beam dimensions corresponding to a beam density of 1.55×10^8 cm^{-3}), and divide by the square of the beam transmission (T = 0.88 through each of two grids) to calculate the measured expelled ion current. Solving for the ionization plus charge exchange cross sections, we obtain

$\sigma_{I+cx} = I_{GIC}/(q\ n_b\ V_{viewed}\ n_0\ v_b\ T^2) = 1.3 \times 10^{-14}\ cm^2$.

This is near, or exceeds, the upper limit of plausible values for the cross section (sum of ionization of gas by beam impact and charge exchange cross sections). We have identified uncertainties in the measurement and in the expected cross section. First, the ionization gauges are not calibrated. Secondly, we need to evaluate the possibility of other mechanisms contributing to the measured current, thereby increasing the inferred cross section; for example, beam-gas photon emission could generate photoelectrons at electrodes and scattered beam ions could cause more electron emission at the electrodes; if electron emission is not completely suppressed by the quadrupole magnetic field, this would increase the current and the inferred ionization cross section. Finally, R. E. Olson has pointed out to us that, although these cross sections appear too large, large charge-exchange cross sections might be reasonable for argon gas — because K^+ ions have the same number of electrons as Ar atoms, making this interaction an effectively resonant charge exchange interaction with correspondingly large cross sections. (Resonant charge-exchange means that the beam ion is of the same element as the gas atom that it impacts so that an exchanged electron can end up in its initial energy state.) He suggests comparing with neon or other gases for which the interaction will definitely be nonresonant [19]. For example, measurements of Ar^+ onto Ar gas at 50-300 keV extrapolate to ionization cross sections at 1 MeV of 2-3 $\times 10^{-15}\ cm^2$ [20]. In future work, we will be addressing these issues.

In summary, we have developed an in-situ fast ionization gauge that (3) measures gas density within an ion beam. It is applicable to space-charge dominated beams with relatively high fill factor, where cold ions can be expelled across the quadrupole magnetic field by the beam potential, and with a beam duration that is longer than the cold ion expulsion time. Despite possible large uncertainties in measuring the cross-section, we have demonstrated an approximately calibrated measurement of gas density within an ion beam. A more accurate calibration can be achieved in the future by calibrating the ion gauges and by using a static gas fill to eliminate the pressure drop across the fourth magnet.

This diagnostic also provides a nearly direct measurement of the generation rate of electrons by beam impact ionization of gas. The measured ion current differs from the electron ionization rate because charge exchange produces a cold ion, but no electron. In general in our energy range, charge exchange cross sections are smaller than ionization cross sections, particularly for non-resonant interactions. Therefore, we expect the electron ionization rate to be within a factor of about 2 of the ion expulsion rate.

We analyze the particle balance of electrons,

$dn_e/dt = n_b\ n_0\ v_b\ \sigma_I - n_e / \tau_d$

where the electron lifetime τ_d is the time for an electron to drift the length of a magnet, which can be computed from its drift velocity ($v_{ExB} + v_{\nabla B}$) and the length L of a quadrupole magnet

$\tau_d = L / (v_{ExB} + v_{\nabla B})$.

We recognize that the ExB drift velocity is proportional to the beam potential, which is proportional to the net space charge, so it will decrease if electrons

partially neutralize the beam. Similarly, the □B drift (including curvature drift) depends linearly on the energy of the electrons perpendicular and parallel to the magnetic field, which will also be proportional to the space-charge potential. We therefore multiply $v_d = L/\tau_d$ by the factor $(n_b - n_e)/ n_b$, for which τ_d becomes τ_{d0} to represent the drift time with $n_e = 0$. Eq. 4 then becomes

$$dn_e /dt = n_b n_0 v_b \sigma_I - n_e [(n_b - n_e) / n_b \tau_{d0}] \quad (7a)$$

Solving this in equilibrium ($dn_e /dt = 0$), we obtain a quadratic equation for n_e, which has two roots:

$$n_e / n_b = n_0 v_b \sigma_I \tau_{d0} \leq \text{few } \%, \quad (7b)$$

and

$$n_e / n_b \approx 1.$$

The implication of the first root is that the electron drift velocity rapidly transports electrons out of a quadrupole magnet into a drift region where either a clearing electrode [18] or an acceleration gap can remove the electrons fast enough that they do not build up. The second root has $n_e / n_b \approx 1$ so the beam potential is near zero and the drift velocities are therefore also near zero. This motivates searching for methods of removing electrons from drift regions or from within quadrupole magnets, and for methods of preventing the occurrence of the second root. Simulations have shown that heavy ion beams, in a system of 200 quadrupoles, are robust to prescribed electron distributions of at least several percent of the beam density (up to 20% for random electron densities) [17], which is very encouraging if we can prevent root 7b from occurring. We have demonstrated the effectiveness of positively-biased clearing electrodes for removing essentially all electrons from drift regions [18], and plan future tests of the effectiveness of induction cells for the same purpose. Related work on the Neutralized Transport Experiment (NTX) has demonstrated that positively-biased screens surrounding the beam can reduce electron populations in drift regions and their effect on the size of the beam focal spot [21].

In conclusion, we have demonstrated that rough surfaces are an effective mitigation technique for reducing ion-induced electron emission (~□10) and gas desorption (~□2), and have found that the SRIM code predicts a □20(6) reduction in ion scattering. We demonstrated a diagnostic that measures gas density within the beam and from which we can infer the electron generation and trapping rate due to ionization of gas. Finally, we have found both low and high electron density solutions from a simple particle balance for electrons in positive ion beams.

Acknowledgements

We are grateful to Ralph Hipple, William Strelo, Ron Beggs, Tak Katayanagi, Gary Ritchie, Craig Rogers, and Ed Romero for excellent technical support. This work was performed under the auspices of the U.S. Department of Energy by University of California, Lawrence Livermore National Laboratory under contract No. W-7405-Eng-48, and by University of California, Lawrence Berkeley National Laboratory under Contract DE-AC03-76F00098.

References

[1] http://wwwslap.cern.ch/collective/ecloud02/proceedings/index.html

[2] S. Y. Zhang, "ICFA Workshop on Beam Induced Pressure Rise in Rings," http://www.c-ad.bnl.gov/icfa (2003).

[3] R. O. Bangerter, Phil. Trans. R. Soc. Lond. A **357**, 575 (1999).
[4] A. W. Molvik, R. Cohen, A. Friedman, S. Lund, et al., "Initial Experimental Studies of Electron Accumulation in a Heavy-Ion Beam," Proc. Of the 2003 Particle Accelerator Conference, p. 312 (IEEE, 2003).
[5] R. H. Cohen, A. Friedman, S. M. Lund, A. W. Molvik, M. Furman, J.-L. Vay, and P. Stoltz, Proc. Of the 2003 Particle Accelerator Conference, p. 132 (IEEE, 2003).
[6] A. W. Molvik, M. Kireeff Covo, F. M. Bieniosek, L. Prost, P. A. Seidl, D. Baca, A. Coorey, and A. Sakumi, "Gas desorption and electron emission for 1 MeV potassium ion bombardment of stainless steel," Phys. Rev. Special Topics – Accelerators and Beams **7**, 093202 (2004).
[7] R. Meinke, W. Nexsen, E. Tsyganov, and A. Zinchenko, "Limitations of a Residual Gas Ionization Beam Profile Monitor for the SSC Collider," Proc. Of the 1993 Particle Accelerator Conference, p. 2468 (IEEE, 1993).
[8] V. Variale, N. Ceci, V. Valentino, G. V. Lamanna, T. Clauser,V. Stagno, A. Ainelli, M. Poggi, "First Test Results for a Residual Gas Beam Profile Monitor," Proc. Of the 1997 Particle Accelerator Conference, p. 2169 (IEEE, 1997).
[9] W. C. Sellyey, J. D. Gilpatrick, Ralph Senior, "Bench Test of a Residual Gas Ionization Profile Monitor (RGIPM)," Proc. Of the 2001 Particle Accelerator Conference, p. 1318 (IEEE, 2001).
[10] P. Forck, A. Bank, "Residual Gas Fluorescence for Profile Measurements at the GSI UNILAC," Proc. Of the 2002 European Particle Accelerator Conference, p. 1885 (2002).
[11] Y. Hashimoto, Y. Fujita, T. Morimoto, S. Muto, T. Fujisawa, et al., "Development of a Gas-Sheet Beam Profile Monitor," Proc. Of the 2001 Asian Particle Accelerator Conference, p. 791 (2001).
[12] L. Prost, F. Bieniosek, S. M. Lund, P.A. Seidl, et al., "Experimental Study of the Transport Limits of Intense Heavy-Ion Beams in the High Current Transport Experiment," Paper W.I-07, Proceedings of the 15th International Symposium on Heavy Ion Inertial Fusion, Princeton NJ, June 7-11, 2004.
[13] P. Thieberger, A. L. Hanson, D. B. Steski, V. Zajic, S. Y. Zhang, and H. Ludewig, Phys. Rev. A. **61**, 042901 (2000).
[14] E. Mahner, J. Hansen, J.-M. Laurent, and N. Madsen, Rhys. Rev. Special Topics – Accelerators and Beams **6**, 013201 (2003).
[15] J. F. Ziegler, http://www.srim.org/.
[16] R. H. Cohen, A. Azevedo, A. Friedman, M. A. Furman, S. M. Lund, A. W. Molvik, P. Stoltz, and S. Veitzer, "Simulating Electron Cloud Effects in Heavy-Ion Accelerators, Th.I-03, Proceedings of the 15th International Symposium on Heavy Ion Inertial Fusion, Princeton NJ, June 7-11, 2004.
[17] R.H. Cohen, A. Friedman, S.M. Lund, A.W. Molvik, E.P. Lee, et al. "Electron-cloud simulation and theory for high-current heavy-ion beams" to be published in Rhys. Rev. Special Topics – Accelerators and Beams.
[18] A. W. Molvik, R. H. Cohen, A. Friedman, M. Kireeff Covo, P. A.

Seidl, . M. Bieniosek, A. Faltens, L. Prost, “Experimental Studies of electron and Gas Sources in a Heavy-Ion Beam,” 31st ICFA AdvancedBeamDynamics Workshop on Electron-Cloud Effects “ECLOUD’04”, Napa, CA, USA, April 19-23, 2004. Available at http://icfa-ecloud04.web.cern.ch/icfa-ecloud04/.

[19] R. E. Olson, private communication (June, 2004).

[20] R. K. Cacak, and T. Jorgensen, Jr., Phys. Rev. A **2**, 1322 (1970).

[21] P. K. Roy, S. S. Yu, S. Eylon, E. Henestroza, A. Anders, et al., Phys. Plasmas **11**, 2890 (2004).

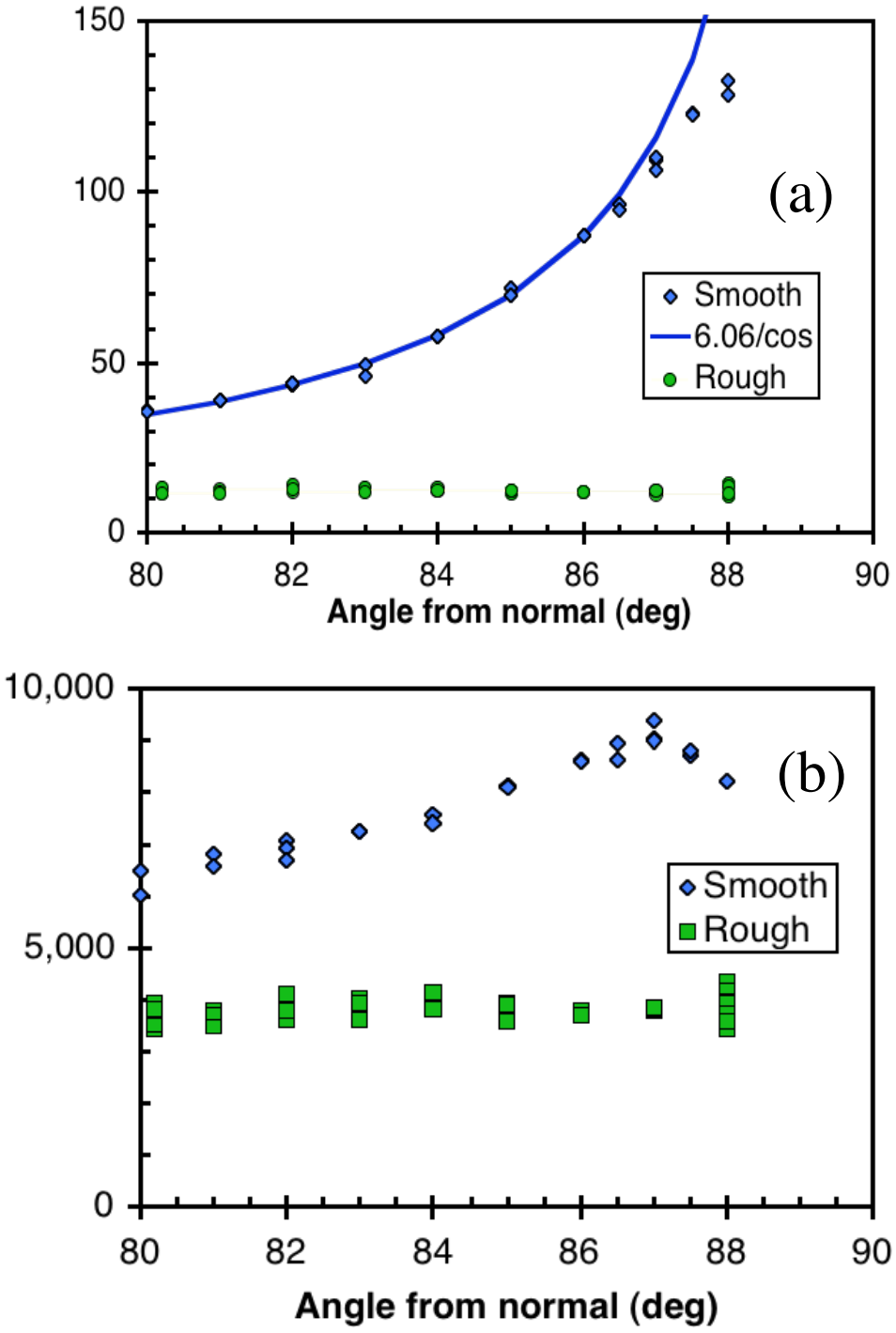

Fig. 1. (a) Electron emission coefficient as a function of angle of incidence, measured from normal to the smooth stainless steel target. [blue-diamonds] The blue line, given by 6.06/cos(□), is a fit to the data between 80° and 86°. [Green circles] Data from a stainless steel surface roughened by bead blasting. (b) [blue diamonds] Gas desorption coefficient data from a smooth stainless steel surface; [green squares] similar data from a bead-blasted surface.

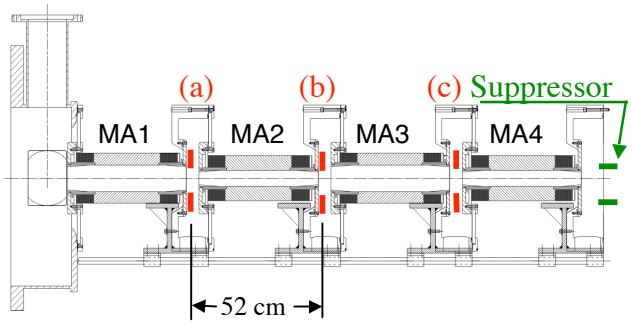

Fig. 2. Magnetic quadrupole region of HCX, from the D2 diagnostic region on the left to the D-End diagnostic region beginning on the right. The half lattice length is 0.52 m. Clearing electrodes a, b, and c are shown in the drift regions between each pair of quadrupoles. A suppressor electrode prevents beam induced electron emission, from structures hit by beam in D-End, from reaching the quadrupole magnets. Diagnostics are mounted on the outside of octagonal tubes, within the bores of the third and fourth magnets, and are either flush with, or recessed behind, the inner wall of the octagonal tubes.

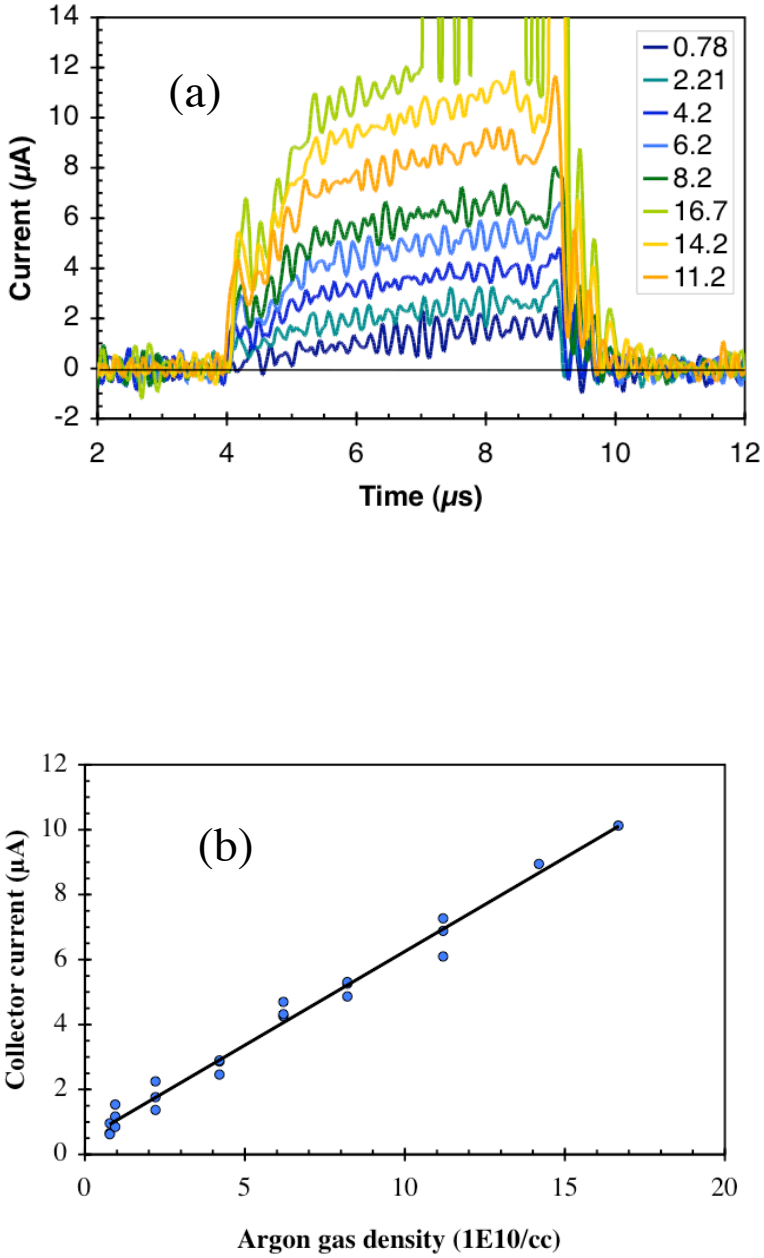

Fig. 3. (a) Current to a grid-shielded electrode versus time. The legend gives the gas density in units of 10^{10} cm^{-3}, calculated from ion gauge measurements as described in text. (b) The initial current increases linearly with the background pressure, which is varied by injecting argon gas, indicating that it provides a measurement of gas density in the ion beam within a magnetic quadrupole.